Journal of the Korean Physical Society, Vol. 46, No. 4, April 2005, pp. 861∼866

Predictive Numerical Simulations on the Formation of Internal Transport Barriers in the Reversed Shear Regime of KSTAR Tokamak

Sun Hee Kim,* Jin Myung Park and Sang Hee Hong
Department of Nuclear Engineering, Seoul National University, Seoul 151-742

(Received 13 October 2004, in final form 23 December 2004)

Numerical simulations have been carried out to predict the formation of internal transport barriers (ITBs) in the reversed shear (RS) regime of Korea Superconducting Tokamak Advanced Research (KSTAR) tokamak by using the ASTRA-1.5D transport code coupled with a simplified neutral beam injection (SINBI) code developed for this work. The present simulations employ a multi-mode transport model, MMM95, for anomalous transport calculations and use neutral beam injection for additional plasma heating and current drive. The simulations for the KSTAR plasmas reveal that ITBs are formed in the RS regime by control of $\mathbf{E} \times \mathbf{B}$ flow shear and by very low magnetic shear, and steep gradient regions apparently reside in both the ion and the electron temperature profiles. Suppression of plasma transport has been considered in this work in two ways: control of the coefficient deciding the strength of $\mathbf{E} \times \mathbf{B}$ flow shearing rate and addition of the effect of magnetic shear to the flow shear.

PACS numbers: 52.65. -y, 52.55.Fa, 52.50.Gj
Keywords: KSTAR tokamak, Internal transport barrier, Reversed shear regime, Numerical simulation

I. INTRODUCTION

Among the improvements in plasma confinement performance observed in many worldwide tokamak devices since the 1990's [1–3], a reversed shear (RS) or negative central shear (NCS) regime is one of the most attractive concepts to prepare for the next generation burning plasma experiments. Therefore, most present major tokamaks have been devoted to the study of this operation regime as an advanced tokamak (AT) operation. In this respect, the Korea Superconducting Tokamak Advanced Research (KSTAR) tokamak, which is being built at the Korea Basic Science Institute (KBSI), also aims to reach the RS regime through a non-inductive current drive in its AT operation [4]. The RS regime is characterized by a negative or very low central magnetic shear region, and reduced thermal transports to near neoclassical values and reduced particle transport have been observed in this regime. The reduction in the transports, caused by an internal transport barrier (ITB) formed in the core plasma of the tokamak, is related to the stabilization of micro-turbulences due to sheared $\mathbf{E} \times \mathbf{B}$ flow and negative or very low magnetic shear [5]. Therefore, reproducing or predicting the ITB plasma through numerical simulations requires plasma transport models based on micro-turbulence suppression physics. In the present numerical work, a multi-mode transport model, MMM95 [6,7] of the National Transport Code Collaboration (NTCC) Module Library, has been employed to simulate the ITB formation in the RS regime of the KSTAR tokamak. In order to establish an RS configuration in the KSTAR tokamak plasma, we use neutral beam injection (NBI) as an additional plasma heating and current drive method. The profiles of the heating power and the current driven by NBI in the tokamak plasma are calculated by using a simplified neutral beam injection (SINBI) code which has been developed for this work [8]. The SINBI code includes the drift orbits of fast ions to take into account the direction and the losses of the injected neutral beam. The plasma elongation and triangularity and the multi-step ionization (MSI) effect are also included in the computations of the profiles in order to get more accurate results. The steady-state Fokker-Planck solution is used to calculate the neutral-beam-driven current profiles [8]. The SINBI module is coupled with the ASTRA-1.5D transport code [9] for numerical simulations on the RS regime of the KSTAR tokamak. Suppression of plasma transport has been considered in this simulation work in the following two ways: i) control of the coefficient deciding the strength of $\mathbf{E} \times \mathbf{B}$ flow shearing rate in the MMM95 model and ii) inclusion of the effect of a very low magnetic shear in the presence of an $\mathbf{E} \times \mathbf{B}$ flow shear.

II. TRANSPORT MODEL AND SIMULATION PROCEDURE

*E-mail: ksunhee8@fusma.snu.ac.kr; Fax: +82-2-877-1343

The MMM95 transport model used as the main anomalous transport model and the Galeev-Sagdeev transport model used as a neoclassical transport model [10] result in the electron and the ion thermal diffusivities and the particle diffusivity as follows:

$$\chi_e = \chi_e^{mmm95} + \chi_e^{neoclassical} \tag{1}$$

$$\chi_i = \chi_i^{mmm95} + \chi_i^{neoclassical} \tag{2}$$

$$D = D^{mmm95} \tag{3}$$

The MMM95 transport model includes the ion temperature gradient (ITG) and the trapped electron mode (TEM) in the Weiland model [11–13], the resistive ballooning mode [14, 15], and the kinetic ballooning mode. Throughout the present numerical simulations, the ten-equation version of the Weil and model and the super-shot setting of the kinetic ballooning mode in the MMM95 transport model have been used. The suppression of micro-turbulence occurs when the $\mathbf{E}\times\mathbf{B}$ flow shearing rate, ω_s, is greater than the maximum growth rate γ of the drift modes [5]. In the MMM95 transport model, a reduction of plasma transport by $\mathbf{E}\times\mathbf{B}$ flow shear is implemented by using a reduced growth rate, $\gamma - C_s\omega_s$, in the calculation of the turbulent transport coefficients. The strength of the $\mathbf{E}\times\mathbf{B}$ flow shearing rate is controlled by a coefficient C_s, and its value can be determined through tokamak experiments and can be varied in accordance with the tokamak device. Therefore, the coefficient values should be carefully selected for the predictive simulations.

The $\mathbf{E}\times\mathbf{B}$ flow shearing rate ω_s is given by [5]

$$\omega_s = \left| \frac{RB_\theta}{B_\phi}\frac{\partial}{\partial r}\left(\frac{E_r}{RB_\theta}\right)\right| \tag{4}$$

where r, R, B_θ, B_ϕ and E_r are the minor radius, the major radius, the poloidal magnetic field, the toroidal magnetic field, and the radial electric field, respectively. The radial electric field is obtained from the toroidal and the poloidal rotations and the ion pressure gradients by [5]

$$E_r = u_{\phi i}B_\phi - u_{\theta i}B_\phi + \frac{1}{Z_i e n_i}\frac{dp_i}{dr} \tag{5}$$

where $u_{\theta i}$ and $u_{\phi i}$ are the poloidal and the toroidal rotation velocities of the ions, respectively. Z_i, e, n_i and p_i are the ion charge number, the electron charge, the ion density and the ion pressure, respectively. The toroidal rotation velocity is calculated from the toroidal momentum conservation Equation [16]:

$$\frac{\partial m_i n_i u_{\phi i}}{\partial t} = -\nabla\left(-m_i n_i \chi_\phi \frac{\partial u_{\phi,i}}{\partial r}\right) + S \tag{6}$$

where m_i, χ_ϕ and S are the ion mass, the toroidal momentum diffusivity, and the toroidal momentum source, respectively. The toroidal momentum diffusivity is set to $1.5\chi_i$ and the toroidal momentum source is computed in the SINBI module with a simple assumption that the total momentum transferred from the neutral beam is conserved in the plasma [8]:

$$S = \frac{n_i m_i u_{\phi i}}{\tau_\phi} = \frac{n_f m_f \nu_f}{\tau_f}\frac{\mathbf{v}_f\cdot\hat{\mathbf{b}}}{\nu_f} \tag{7}$$

where $\tau_\phi, n_f, m_f, \nu_f, \tau_f$ and $\boldsymbol{\nu}_f\cdot\hat{\boldsymbol{b}}/\nu_f$ are the momentum confinement time, the fast ion density, the fast ion mass, the fast ion velocity, the fast ion lifetime, and the pitch angle, respectively. The poloidal rotation velocity is obtained by using the neoclassical formula [17]. However, the $\mathbf{E}\times\mathbf{B}$ flow shearing rate calculated by using Eqs. (4) and (5) is more applicable to circular cross-sec tional plasmas, and its value is usually very large in the outer plasma region. Therefore, in order to reflect the real plasma shape in the calculation following the method used in the GLF23 transport model [18], we use multiplier $\alpha_e = 0.6$ and an effective magnetic field $B_{unit} = B_0\rho d\rho/rdr$ for the calculation of the $\mathbf{E}\times\mathbf{B}$ flow shearing rate, where ρ is defined as $\sqrt{\Phi/\pi B_0}$with Φ being the toroidal flux and r the minor radius at the flux surface.

The magnetic shear effect has also been included in this simulation work by introducing a control function $f(s)$ when the magnetic shear s is given by $s = (dq/dr)/(q/r)$, where q is the safety factor. The MMM95 transport model takes into account the magnetic shear, but it assumes that the magnetic shear is greater than 0.5 everywhere in the plasma region. Thus, the effect of very low magnetic shear is not actually included in this model. The control function $f(s)$ is introduced to express suppression of plasma transport by multiplying the anomalous thermal diffusivities $\chi_{e,i}^{mmm95}$ by the value of $f(s)$ in the region where the magnetic shear is very low:

$$f(s) = \frac{1}{1+C_m e^{-10(s-0.25)}} + \frac{1}{1+C_m e^{10(s+0.25)}} \tag{8}$$

where C_m is the control coefficient and determines the suppression strength of plasma transport by the magnetic shear s. For the same reason mentioned in the selection of C_s for the $\mathbf{E}\times\mathbf{B}$ flow shear, the control coefficient C_m for the magnetic shear should be carefully decided for predictive simulations. In this simulation work, the values of C_m have been chosen as 2.0 and 10.0 to see the effect of magnetic shear.

In the present numerical simulations, the total plasma current is assumed to increase at a constant rate for the first 3 seconds up to its saturation value. Electron and ion densities also evolve according to the prescribed volume-averaged electron density and effective charge number. The volume-averaged electron density is assumed to be sufficiently low to form an ITB plasma in the KSTAR tokamak. The plasma and the impurity ions are assumed to be deuterium and carbon, respectively,

Table 1. KSTAR tokamak discharge parameters used for the RS regime simulations.

Parameter	Value
Major radius R_0	1.8 m
Minor radius a	0.5 m
Triangularity δ	0.5
Elongation κ	2.0
Plasma current I	1.5 MA
Toroidal magnetic field B_0	2.5 T
Plasma ions	Deuterium
Impurity ions	Carbon
Effective charge Z_{eff}	2.0

Table 2. Neutral beam parameters used for the RS regime simulations of KSTAR tokamak.

Parameter	Value
Number of beam lines	2
Beam energy, E_{NB}	120 keV
Beam power, P_{NB}	Not fixed (MW)
E : E/2 : E/3	0.67 : 0.19 : 0.14
Beam shape	Rectangular
Beam size (w, h)	(0.36, 0.70)
Gaussian half-width (σ_R, σ_Z)	(0.18, 0.35)
Beam central position	
Beam 1 (R_t, Z_t)	(1.8, 0.0)
Beam 2 (R_t, Z_t)	(1.55, 0.0)

and the effective charge number is set to 2.0 everywhere in the tokamak plasma. Two neutral beams are injected from the current ramp-up phase, and their total power reaches 10.67 MW. To build an RS configuration in the KSTAR tokamak, neutral-beam-driven currents are carefully applied to achieve hollow profiles through the three time-steps during the current ramp-up phase because the current ramp-up rates of its superconducting coils are too slow to adopt a conventional fast current ramp-up method with an intense central heating. The values of the parameters for the KSTAR tokamak discharge and the neutral beams [19] used for the RS regime simulations are listed in Tables 1 and 2.

III. SIMULATION RESULTS AND DISCUSSION

First, the effect of $\mathbf{E} \times \mathbf{B}$ flow shear on the RS regime of the KSTAR tokamak has been examined without the inclusion of a very low magnetic shear. The coefficient C_s for controlling the strength of the $\mathbf{E} \times \mathbf{B}$ flow shear is set to 1.0, and the control function $f(s)$ for the magnetic shear effect is not applied to the anomalous thermal diffusivities. Time traces of the numerical simulation are

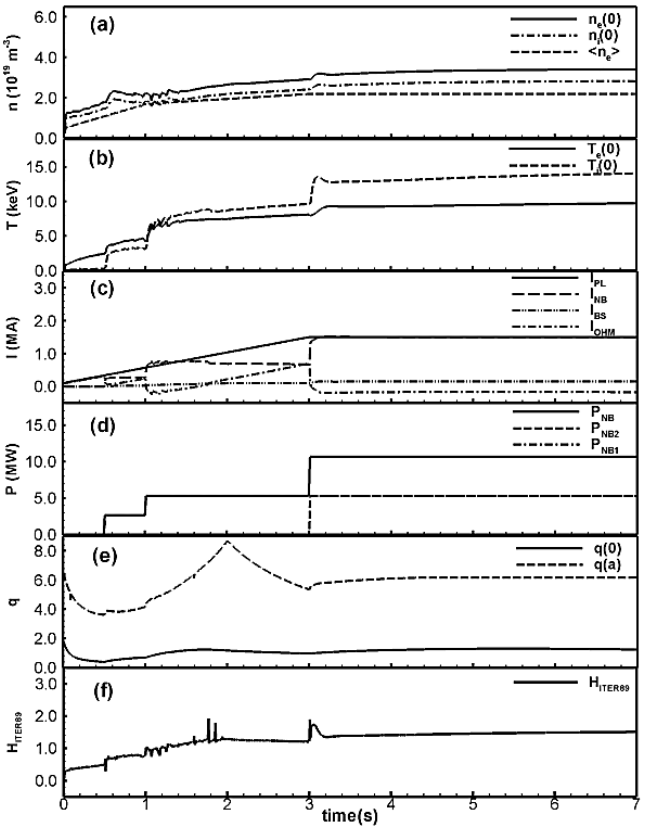

Fig. 1. Time traces of (a) plasma densities, (b) plasma temperatures, (c) plasma currents, (d) injected neutral beam powers, (e) safety factors, and (f) confinement enhancement factor observed in the numerical simulations on the RS regime of the KSTAR tokamak with only the effect of $\mathbf{E} \times \mathbf{B}$ flow shear ($C_s = 1.0$) considered.

shown in Fig. 1, in which the plasma densities, temperatures, and neutral-beam-driven current respond to the change of neutral beam power, and the central safety factor $q(0)$ increases to over 1.0 due to the hollow current profile produced by the NBI. The confinement enhancement factor H_{ITER89} also increases with the NBI power.

Figure 2 shows various radial profiles as functions of the normalized toroidal flux ρ_T. In Fig. 2(a), the central ion temperature increases up to 13.5 keV at 3.12 s during the discharge, and the steep gradient regions of the temperature are shifted radially outward, indicating an expansion of the enhanced confinement region during the neutral-beam power increase from 5.33 MW to 10.67 MW at 3.0 s. Unexpectedly, the ion temperature profile at 2.91 s already has a sufficiently steep slope region in spite of the lower power of NBI. This is due to the supershot setting of the MMM95 transport model used at the beginning of this numerical simulation. A quite steep gradient region also appears in the electron temperature profile, but it is not seen in the electron density profile in Fig. 2(b). In the steep temperature gradient region near $\rho_T = 0.47$, the thermal diffusivities are reduced by

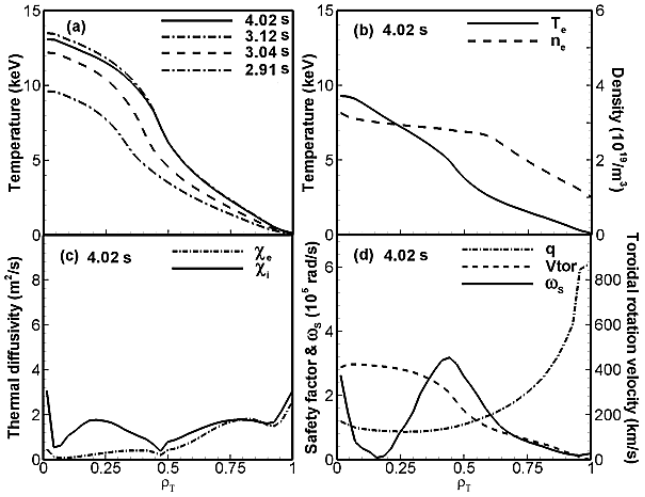

Fig. 2. Radial profiles as functions of the normalized toroidal flux ρ_T for (a) the ion temperatures at different discharge times, (b) the electron temperature and density, (c) the ion and the electron thermal diffusivities, and (d) the safety factor, the toroidal rotation velocity, and the $\mathbf{E} \times \mathbf{B}$ flow shearing rate at t = 4.02 s, as predicted by the numerical simulations on the RS regime of the KSTAR tokamak with only the effect of $\mathbf{E} \times \mathbf{B}$ flow shear ($C_s = 1.0$) considered.

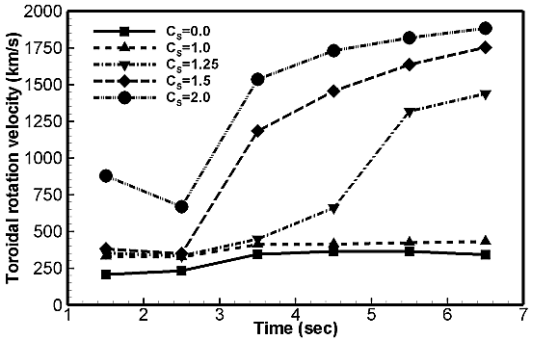

Fig. 3. Temporal toroidal rotation velocities at the central region obtained from the RS regime simulations for the KSTAR tokamak with various $\mathbf{E} \times \mathbf{B}$ flow shearing rates.

the $\mathbf{E} \times \mathbf{B}$ flow shear applied through its shearing rate ω_s, as shown in Figs. 2(c) and (d).

During the numerical simulations, a positive feedback mechanism related to the formation of the ITB is observed. Application of a strong $\mathbf{E} \times \mathbf{B}$ flow shear suppresses plasma transports; then, this suppression causes the toroidal plasma rotation to increase in the reduced transport region. The increase in the toroidal velocity changes the radial electric field and reinforces the $\mathbf{E} \times \mathbf{B}$ flow shear in return. However, this positive feedback mechanism stops at a certain level as a result of competition between the suppression mechanism and another transport enhancement mechanism in which the maximum growth rate of drift modes is increased by the steep pressure gradients. Consequently, a new state with steep temperature gradients is generated by this competition as the ITB is formed in the plasma region.

As mentioned earlier, the control coefficient C_s for the strength of the $\mathbf{E} \times \mathbf{B}$ flow shearing rate should be chosen carefully for predictive simulations. In fact, a higher value of C_s could lead to a stronger ITB and a higher central plasma temperature. However, for reproduction and prediction of an ITB plasma, unreasonable values of the $\mathbf{E} \times \mathbf{B}$ flow shearing rate could generate physically unacceptable results. To find an appropriate value for the coefficient C_s, we performed additional numerical simulations to investigate the temporal behavior of the central toroidal rotation velocity, and the results are plotted in Fig. 3 for different shearing rates controlled by C_s. Though a simple method is used to calculate the toroidal rotation velocity driven by NBI, a comparison among the resultant toroidal velocities provides an appropriate range for the coefficient C_s, which makes it possible to simulate the ITB formation and gives some clues for explaining the formation process. In Fig. 3, values of coefficient C_s over 1.25 are seen to produce very high toroidal rotation velocities after full-power injection of the neutral beam at 3.0 second. In view of a thermal velocity of about 1400 km/s for deuterium ions at a temperature of 20 keV, these calculated toroidal rotation velocities are unreasonably high. Therefore, the appropriate range for the coefficient C_s in this simulation condition turns out to be about $1.0 \sim 1.15$. The causes of excessively high toroidal rotation velocities being generated for the larger C_s values are not obvious in these simulations, but the broad electron density profile shown in Fig. 2(b), which is expected to have a steep gradient region near the ITB, could be one of them. This question might be answered by using more accurate particle transport models.

The effect of very low magnetic shear on ITB formation has been examined by introducing the control function $f(s)$ to the previous simulations for the $\mathbf{E} \times \mathbf{B}$ flow shear. Weak ($C_m = 2.0$) and strong ($C_m = 10.0$) magnetic shears are added to the $\mathbf{E} \times \mathbf{B}$ flow shear ($C_s = 1.0$), respectively, and the simulation results are drawn in Figs. 4(a) and 4(b). In the upper figures for the ion and the electron temperature profiles, the dotted lines represent the previous results obtained without the magnetic shear effect, as presented in Figs. 2(a) and 2(b). The profiles calculated in the presence of the $\mathbf{E} \times \mathbf{B}$ flow shear effect only are plotted here to compare their temperature variations with those obtained by inclusion of the magnetic shear effect. In both the numerical simulations, plasma transport is suppressed by the magnetic shear only near the central plasma region. As Fig. 4(b) shows, the strong magnetic shear gives rise to a great increase in the central ion temperature and a slight decrease in the thermal diffusivities near the central region. In addition, the central safety factor is increased slightly, and the $\mathbf{E} \times \mathbf{B}$ flow shearing rate is larger with its profile being broadened radially inward. This expanded profile of the flow shearing rate can be explained by using

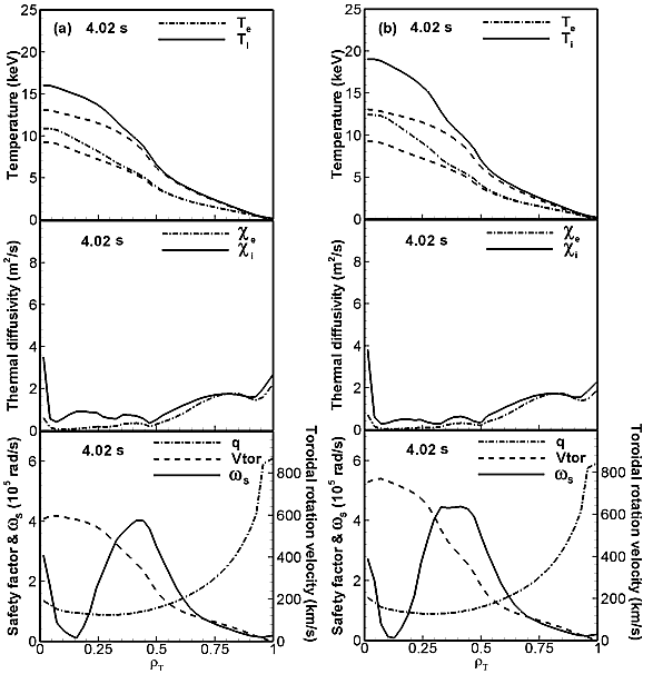

Fig. 4. Radial profiles as functions of the normalized toroidal flux ρ_T for the ion and the electron temperatures, their thermal diffusivities, the safety factor, the $\mathbf{E} \times \mathbf{B}$ flow shearing rate, and the toroidal rotation velocity, as predicted by the numerical simulations on the RS regime of the KSTAR tokamak operated with (a) a weak magnetic shear of $C_m = 2.0$ and (b) a strong magnetic shear of $C_m = 10.0$ in the presence of $\mathbf{E} \times \mathbf{B}$ flow shear ($C_s = 1.0$). The dotted lines in the upper sections of (a) and (b) represent the ion and the electron temperatures obtained without consideration of the magnetic shear effect considered in Figs. 2 (a) and (b).

a mechanism similar to the previous positive feedback mechanism. The ion thermal diffusivity is reduced by the magnetic shear and causes the toroidal rotation velocity to increase in the very low magnetic shear region; then, the increased toroidal velocity strengthens the $\mathbf{E} \times \mathbf{B}$ flow shearing rate in that region. This implies that there could be some coupling between the $\mathbf{E} \times \mathbf{B}$ flow shear and the magnetic shear. However, at present, it is an open question whether these reductions of plasma transports by the two shears occur independently or not.

IV. CONCLUSION

In this predictive numerical work, the formation of ITBs in the RS regime of the KSTAR tokamak is simulated by using the ASTRA-1.5D transport code coupled with the SINBI module and the MMM95 transport model based on ITG and TEM physics. The characteristics of ITBs appear clearly in the ion temperature and thermal diffusivity profiles. The plasma temperature profiles predicted in the numerical simulations have steep gradients near the central plasma region, and the steep gradient region shifts radially outward when the neutral beam power is increased.

The effects of an $\mathbf{E} \times \mathbf{B}$ flow shear and a very low magnetic shear on the anomalous plasma transport have been examined. Plasma transport is strongly suppressed by the $\mathbf{E} \times \mathbf{B}$ flow shear where its shearing rate is peaked. From the competition between the suppression and the enhancement mechanisms of plasma transport, a new plasma state is generated with steep temperature gradients, indicating the formation of an ITB near the peak of the $\mathbf{E} \times \mathbf{B}$ flow shearing rate.

The effect of a very low magnetic shear is simulated by using the control function $f(s)$ in the presence of an $\mathbf{E} \times \mathbf{B}$ flow shear. When a strong magnetic shear effect is applied, an expanded profile of the $\mathbf{E} \times \mathbf{B}$ flow shearing rate is observed, which suggests that the suppression of plasma transport by the magnetic shear leads to the compensating effect of an increased $\mathbf{E} \times \mathbf{B}$ flow shearing rate. Though the strengths of the $\mathbf{E} \times \mathbf{B}$ flow shear and the magnetic shear should be decided carefully for predictive numerical simulations, by selecting appropriate values, we have successfully simulated ITB formation in the RS regime of the KSTAR tokamak. This simulation work should provide some useful experimental hints and expected data for advanced tokamak operation of the KSTAR tokamak.

ACKNOWLEDGMENTS

This work was supported by the Korea Basic Science Institute in Korea.

REFERENCES

[1] R. J. Groebner, Phys. Fluids B **5**, 2343 (1993).
[2] E. A. Lazarus, L. L. Lao, T. H. Osborne, T. S. Taylor, A. D. Turnbull, M. S. Chu, A. G. Kellman, E. J. Strait, J. R. Ferron, R. J. Groebner, W. W. Heidbrink, T. Carlstrom, F. J. Helton, C. L. Hsieh, S. Lippmann, D. Schissel, R. Snider and D. Wroblewski, Phys. Fluids B **4**, 3644 (1992).
[3] M. Hugon, B. Ph. van Milligen, P. Smeulders, L. C. Appel, D. V. Bartlett, D. Boucher, A. W. Edwards, L. -G. Eriksson, C. W. Gowers, T. C. Hender, G. Huysmans, J. J. Jacquinot, B. J. D. Tubbing, M. L. Watkins, W. Zwingmann, Nucl. Fusion **40**, 575 (2000).
[4] G. S. Lee, J. Kim, S. M. Hwang, C. S. Chang and H. Y. Chang, *et al.* Nucl. Fusion **40**, 575 (2000).
[5] R. C. Wolf, Plasma Phys. Control. Fusion **45**, R1 (2003).
[6] G. Bateman, A. H. Kritz, J. E. Kinsey, A. J. Redd and J. Weiland, Phys. Plasmas **5**, 1793 (1998).
[7] P. Zhu, G. Bateman, A. H. Kritz and W. Horton, Phys. Plasmas **7**, 2892 (2000).
[8] S. H. Kim, M.S. Thesis, (Seoul National University, Seoul, 2004).

[9] G. V. Pereverenzev and P. N. Yushmanov, Report IPP 5/98 (2002).
[10] M. Ju, J. Kim and KSTAR Team, Nucl. Fusion **40**, 1859 (2000).
[11] H. Nordman, J. Weiland and A. Jarmen, Nucl. Fusion **30**, 983 (1990).
[12] J. Weiland and A. Hirose, Nucl. Fusion **32**, 151 (1992).
[13] J. Nilsson and J. Weiland, Nucl. Fusion **34**, 803 (1994).
[14] J. E. Kinsey, G. Bateman, A. H. Kritz and A. Redd, Phys. Plasmas **3**, 561 (1996).
[15] P. N. Guzdar, J. F. Drake, D. McCarthy and A. B. Hassam, Phys. Fluids B **5**, 3712 (1993).
[16] K. Nagashima, Y. Koide and H. Shirai, Nucl. Fusion **34**, 449 (1994).
[17] G. M. Staebler, R. E. Waltz and J. C. Wiley, Nucl. Fusion **37**, 287 (1997).
[18] R. E. Waltz and R. L. Miller, Phys. Plasmas **6**, 4265 (1999).
[19] J.-S. Ko, D.-K. Kim and S. H. Hong, J. Korean Phys. Soc. **41**, 212 (2002).